Journal of Cerebral Blood Flow & Metabolism (2015) 35, 1764–1770
© 2015 ISCBFM All rights reserved 0271-678X/15 $32.00
www.jcbfm.com

ORIGINAL ARTICLE

Parkinson's disease–related spatial covariance pattern identified with resting-state functional MRI

Tao Wu[1,2,4], Yilong Ma[3,4], Zheng Zheng[1,2], Shichun Peng[3], Xiaoli Wu[1,2], David Eidelberg[3] and Piu Chan[1,2]

In this study, we sought to identify a disease-related spatial covariance pattern of spontaneous neural activity in Parkinson's disease using resting-state functional magnetic resonance imaging (MRI). Time-series data were acquired in 58 patients with early to moderate stage Parkinson's disease and 54 healthy controls, and analyzed by Scaled Subprofile Model Principal Component Analysis toolbox. A split-sample analysis was also performed in a derivation sample of 28 patients and 28 control subjects and validated in a prospective testing sample of 30 patients and 26 control subjects. The topographic pattern of neural activity in Parkinson's disease was characterized by decreased activity in the striatum, supplementary motor area, middle frontal gyrus, and occipital cortex, and increased activity in the thalamus, cerebellum, precuneus, superior parietal lobule, and temporal cortex. Pattern expression was elevated in the patients compared with the controls, with a high accuracy (90%) to discriminate the patients from the controls. The split-sample analysis produced a similar pattern but with a lower accuracy for group discrimination in both the derivation (80%) and the validation (73%) samples. Our results showed that resting-state functional MRI can be potentially useful for identification of Parkinson's disease–related spatial covariance patterns, and for differentiation of Parkinson's disease patients from healthy controls at an individual level.

Journal of Cerebral Blood Flow & Metabolism (2015) **35,** 1764–1770; doi:10.1038/jcbfm.2015.118; published online 3 June 2015

Keywords: biomarker; disease-related spatial covariance pattern; Parkinson's disease; resting-state fMRI; SSMPCA

INTRODUCTION

Parkinson's disease (PD) is a common neurodegenerative disorder. The diagnosis of PD is based mainly on clinical assessments but the diagnostic accuracy is low during early stages of PD.[1] There is an increasing interest in finding viable biomarkers that can be reliably used in identifying at risk individuals, aiding early differential diagnosis, measuring disease progression, and monitoring treatment effects in patients with PD.

Previous neuroimaging studies with ^{18}F-fluorodeoxyglucose (FDG) positron emission tomography (PET) and multivariate network analysis have shown that PD is associated with a specific disease-related spatial covariance pattern (PDRP) of regional cerebral glucose metabolism.[2,3] The expression of PDRP network can be quantified prospectively with FDG PET in individual subjects to distinguish PD patients from healthy controls,[4–6] correlate with independent measures of disease severity,[4] evaluate modulations by novel experimental therapeutics,[5,6] and discriminate PD patients from patients with multiple system atrophy or progressive supranuclear palsy.[7,8] PDRP can also be reliably assessed by imaging regional cerebral blood flow with other radiotracer techniques (PET and SPECT)[2,9] and perfusion magnetic resonance imaging (MRI).[10,11]

Functional MRI (fMRI) has been used to show changes in neural activity[12–14] and connectivity in the resting state in PD patients.[15–18] Regional differences in low-frequency fMRI signal in the resting state were also reported to be reliable for discriminating PD patients from healthy controls.[13] These findings show that resting-state fMRI (rsfMRI) can be used to reveal the distribution of PD-related neural activity and assess its correlations with clinical symptoms. However, the majority of rsfMRI studies was based chiefly on the group-level statistics and is less helpful in prospective clinical applications with individual subjects. In this study, we sought to identify an analogous spatial covariance pattern of spontaneous neural activity in PD using rsfMRI, and examine if this method can be potentially used to discriminate PD patients from healthy controls at an individual level.

SUBJECTS AND METHODS

Subjects

We investigated 58 patients with idiopathic PD (age 61.4 ± 9.0 years, range 45 to 78 years; 25 women, 33 men). The diagnosis of PD was based on medical history, physical and neurologic examinations, response to levodopa, and laboratory tests and MRI scans to exclude other diseases. All patients presented motor symptoms of rigidity and bradykinesia at early to moderate stages but were chosen to have at most a mild tremor to avoid the disturbance of fMRI signal. The Unified Parkinson's Disease Rating Scale (UPDRS)[19] motor score at off state was 24.8 ± 8.2. The Hoehn and Yahr disability scale[20] was 2.0 ± 0.6. All patients had participated in a recent

[1]Department of Neurobiology, Beijing Institute of Geriatrics, Xuanwu Hospital, Capital Medical University, Beijing, China; [2]Beijing Key Laboratory on Parkinson's Disease, Parkinson Disease Center of Beijing Institute for Brain Disorders, Beijing, China and [3]Center for Neurosciences, The Feinstein Institute for Medical Research, The North Shore-Long Island Jewish Health System, Manhasset, New York, USA. Correspondence: Professor T Wu, Department of Neurobiology, Beijing Institute of Geriatrics, Xuanwu Hospital, Capital Medical University, Beijing 100053, China or Professor Y Ma, Center for Neurosciences, The Feinstein Institute for Medical Research, Manhasset, NY 11030, USA.
E-mail: wutao69@gmail.com or yma@nshs.edu
This work was supported by The Michael J. Fox Foundation Rapid Response Innovation Awards, grants from the National Science Foundation of China (81071012 and 81271429), and Seed Grant of International Alliance of Translational Neuroscience (PXM2014_014226_000015). YM, SP, and DE were supported by the NIH Morris K Udall Center of Excellence for Parkinson's Disease Research (P50 NS071675) at The Feinstein Institute for Medical Research.
[4]These authors contributed equally to this work.
Received 13 January 2015; revised 1 May 2015; accepted 8 May 2015; published online 3 June 2015

study.[21] The control group included 54 age- and gender-matched healthy subjects (age 61.1 ± 9.4 years, range 45 to 78 years; 26 women, 28 men). Mini-Mental State Examination was ⩾ 26 in all subjects, with no differences between the patients and the controls. The primary analysis of network identification was performed in these PD patients and healthy subjects defined as cohort A. For the secondary analysis of network validation, subjects in cohort A were randomly divided into a derivation sample (cohort B) of 28 PD patients (age 59.9 ± 9.1 years, Hoehn and Yahr 1.9 ± 0.6, and motor UPDRS 24.2 ± 7.9) and 28 normal controls (age 63.7 ± 9.6 years), and a prospective validation sample (cohort C) of 30 PD patients (age 62.7 ± 8.9 years, Hoehn and Yahr 2.0 ± 0.5, and motor UPDRS 25.3 ± 8.6) and 26 normal controls (age 58.3 ± 8.4 years). Subject groups in these two cohorts were matched for age and clinical symptoms. The experiments were performed according to the Declaration of Helsinki and were approved by the Institutional Review Board of Xuanwu Hospital in Beijing, China. All subjects gave their written informed consent for the study.

Resting-state Functional Magnetic Resonance Imaging Protocols and Processing

Functional MRI acquisition was performed on a 3 T Magnetom Trio system (Siemens, Erlangen, Germany). Parkinson's disease patients were scanned after their medication had been withdrawn for at least 12 hours. High-resolution anatomic images were acquired with a three dimensional magnetization prepared rapid acquisition gradient echo sequence (repetition time (TR)/echo time (TE) = 2,530/3.39 ms, 128 axial slices, 1.33 mm thickness, and field of view = 256 mm). Functional MRI data were collected with a gradient-echo echo-planar sequence (TR/TE = 2,000/30 ms, flip angle = 90°, 33 axial slices, 3.5 mm thickness, no gap, field of view = 220 mm, and matrix size = 64 × 64). During rsfMRI, subjects were instructed to keep their eyes closed, to remain motionless, and to not to think of anything in particular. The rsfMRI scanning session lasted for 8 minutes.

Functional MRI data were preprocessed using Statistical Parametric Mapping (SPM8, http://www.fil.ion.ucl.ac.uk/spm) and Data Processing Assistant for Resting-State fMRI (DPARSF) V2.0 advanced edition (http://www.restfmri.net). Time-series data were first slice-time corrected and aligned to the first image for motion correction. Each subject's head motion parameters were examined. No subject had more than 1.5 mm maximum translation in *x*, *y*, or *z*, or 1.5° of maximum rotation about the three axes. Functional images of each subject were coregistered to anatomic images and spatially normalized into the standard Montreal Neurological Institute brain space. All images were then resampled into $3 \times 3 \times 3\ mm^3$ voxels, and smoothed with an 8-mm Gaussian kernel. After the linear drift was removed, a temporal filter ($0.01\ Hz < f < 0.08\ Hz$) was also applied to remove very-low-frequency drifts and physiologic high-frequency noise.[22]

To identify a specific pattern of neural activity, we analyzed rsfMRI data with the amplitude of low-frequency fluctuation (ALFF) approach, which measures the regional spontaneous activity at rest.[23] Amplitude of low-frequency fluctuation was calculated using the same procedures reported previously,[23] with Resting-State fMRI Data Analysis Toolkit (REST, http://www.restfmri.net). The time courses of all voxels were first converted to the frequency domain using a fast Fourier transform, and the power spectrum was obtained. The square root of the power spectrum was calculated at each frequency and then averaged across 0.01 to 0.08 Hz for each voxel. This averaged square root was taken as an index of ALFF. The ALFF of each voxel was divided by the global mean ALFF value within the brain tissue mask to standardize data across subjects.

Network Analysis

Scaled subprofile model (SSM), which is one of the multivariate spatial covariance techniques based on principal component analysis (PCA), was applied to assess subject-by-voxel effects on ALFF maps in both PD patients and control subjects with Scaled Subprofile Model Principal Component Analysis (SSMPCA) toolbox (http://www.feinsteinneuroscience.org). In contrast to PET or SPECT images, log-transformation was not used for fMRI data because of its additive variability. A PD-related covariance pattern was identified from a linear combination of principal components whose expression in individual subjects maximized the separation between the two groups. This was conducted by logistic regression analysis in the set of contiguous principal components that accounted for ~50% of subject × voxel variance in the SSMPCA operation. The sign of the resultant pattern was defined such that PD patients had elevated mean expression compared with controls. The reliability of this pattern was assessed on a voxel basis by a bootstrapping estimation algorithm.[24] Brain regions deemed reliable from this *post hoc* procedure were localized anatomically in reference to a standard brain atlas in Talairach space (http://www.talairach.org/daemon.html). The primary network analysis used all ALFF images in cohort A. A split-sample analysis was also conducted to identify PDRP again in cohort B and compute its scores prospectively in cohort C to exam the reproducibility of this pattern.

Statistical Analysis

PDRP scores in all subjects were *z*-transformed with regard to the healthy controls in the derivation sample. The resulting scores were compared between the subject groups using Student's two-sample *t*-tests with the discriminating power between the groups evaluated using receiver operating characteristic analysis. The difference in PDRP scores between the gender and their dependence with age were also examined separately in each group. All statistical analyses were performed with SPSS software version 9.0 (SPSS, Chicago, IL, USA) and considered significant at $P < 0.05$.

RESULTS

Parkinson's Disease–Related Covariance Pattern

SSMPCA analysis produced a spatial covariance pattern of neural activity in PD (PDRP–ALFF) characterized by decreased activity in the bilateral caudate nucleus and anterior putamen, bilateral middle frontal gyrus, rostral supplementary motor area (pre-SMA), right lingual and middle occipital gyri, left precuneus and inferior temporal gyrus, and right supramarginal and posterior cingulate gyri, and increased activity in the thalamus, bilateral cerebellum, right medial frontal gyrus/rectus, bilateral precuneus, left superior parietal lobule, and bilateral temporal cortices including posterior insula (Figure 1A and Table 1). This pattern was defined from a set of principal components accounting for a total subject × voxel variance of 34.2% and found to be reliable ($P < 0.025$) over the whole brain based on the bootstrapping algorithm. PDRP–ALFF expression was elevated (Figure 1B; $P < 0.000001$) in the PD patients compared with the controls. Receiver operating characteristic analysis revealed an area under the curve = 0.968 and 95% confidence intervals = 0.94 to 0.99 (Figure 1C) to discriminate the PD patients from the controls. The optimal sensitivity/specificity was 91.4%/88.9% resulting in an accuracy of 90.2% (cutoff value = 1.16; Table 2). In the control subjects, PDRP–ALFF scores were comparable between men and women ($P = 0.563$) and did not correlate with age ($r = 0.22$, $P = 0.11$). In the PD patients, however, PDRP–ALFF scores were moderately greater ($P < 0.05$) in men than in women and correlated weakly ($r = 0.34$, $P < 0.01$) with age.

Reproducibility in the Split Sample

A PD-related spatial covariance pattern of neural activity was produced in cohort B and characterized by decreased activity in the pre-SMA, precuneus, bilateral caudate nucleus, and right lingual and inferior temporal gyri, and increased activity bilaterally in the middle temporal gyrus and cerebellum (Figure 2B). This pattern was defined from a set of principal components accounting for a total subject × voxel variance of 35.3% and found to be reliable ($P < 0.05$) over the whole brain according to the bootstrapping algorithm. Parkinson's disease–related spatial covariance pattern–amplitude of low-frequency fluctuation expression was elevated ($P < 0.001$; Figure 2C) in the PD patients relative to the controls in both the derivation and validation samples. Receiver operating characteristic analyses disclosed an area under the curve of 0.921 (95% confidence intervals = 0.86 to 0.99) and 0.782 (95% confidence intervals = 0.66 to 0.90) in these two samples to discriminate the PD patients from the normal controls leading to a diagnostic accuracy of 80.4% (cutoff value = 0.98) and 69.6% (cutoff value = 0.87), respectively (Figure 2D; Table 2). The use of the cutoff value defined in the derivation sample resulted in a sensitivity/specificity of 66.7%/80.0% and an accuracy of 73.2% in the validation sample.

© 2015 ISCBFM

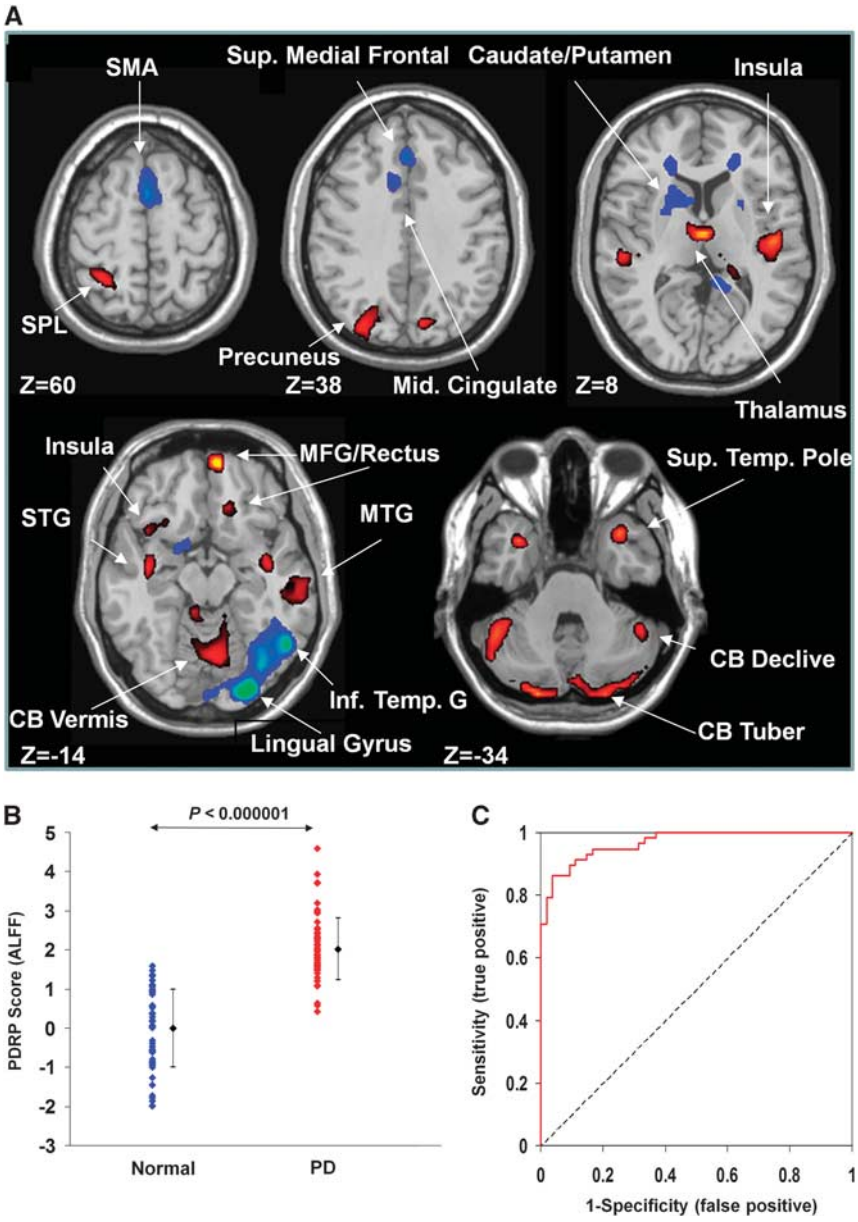

Figure 1. Parkinson's disease–related spatial covariance pattern–amplitude of low-frequency fluctuation (PDRP–ALFF) identified with resting-state functional magnetic resonance imaging (fMRI). (**A**) The pattern was defined using ALFF images from 58 patients with PD and 54 normal controls in cohort A. This network topography was reliable at $P < 0.025$ (see Table 1 for more information). (**B**) Group discrimination by PDRP–ALFF expression in patients with PD and normal controls. The expression of PDRP–ALFF significantly discriminated the PD patients from the normal controls ($P < 0.000001$). (**C**) Receiver operating characteristic curve for discriminating the PD patients from the normal controls. The discriminatory power in cohort A was greater than that in cohort B or cohort C (see Figure 2D). The covariance pattern is superimposed on a standard T1-weighted MRI brain template and displayed with a height threshold of ± 0.5 and an extent threshold of 30 voxels (240 mm^3). Voxels with positive region weights (increased activity) are color-coded *red* and those with negative region weights (decreased activity) are color-coded *blue*. Error bars represent the s.d. plotted around the mean of each subject group. CB, cerebellum; MFG, medial frontal gyrus; MTG, middle temporal gyrus; SMA, supplementary motor area; SPL, superior parietal lobule; STG, superior temporal gyrus.

DISCUSSION

This is the first study that used multivariate SSMPCA methodology to investigate disease-related brain networks in rsfMRI time series. The PD-related spatial covariance pattern we have identified is, to a large part, topographically comparable to the previous results with regional homogeneity,[12] or cross-validation analysis of ALFF in PD patients.[13,14] Although the physiology of fMRI signal is not fully understood, these related studies reveal local and system-level abnormalities in a large number of widely distributed regions and relay stations within the basal ganglia–thalamo–cortical and cerebello–thalamo–cortical circuits.

The PDRP derived from FDG PET is characterized by increased metabolic activity in the posterior putamen, globus pallidus, thalamus, sensorimotor cortex, pons, and cerebellum, along with decreased metabolic activity in the premotor, SMA, and parietooccipital association cortices.[25,26] Compared to the PDRP from FDG PET, the PDRP derived from rsfMRI not only shows some

© 2015 ISCBFM

Table 1. Anatomic regions of PDRP–ALFF derived from resting-state fMRI

Brain region	*MNI coordinates*			*Peak value*	*Cluster size (mm^3)*
	x	y	z		
Decreased activity					
L caudate nucleus	−6	3	12	3.11	1,350
R caudate nucleus	9	−3	18	2.78	756
L anterior putamen	−21	9	3	0.97	2,754
R anterior putamen	25	11	−4	0.59	1,107
L middle frontal gyrus (BA 8)	−27	18	51	1.39	729
L middle frontal gyrus (BA 10)	−30	51	21	1.49	540
R middle frontal gyrus (BA 46)	48	33	18	1.65	729
R supplementary motor area (BA 6)	2	12	51	3.10	11,232
L precuneus (BA 7)	−6	−66	63	4.03	567
R lingual (BA 18)	24	−93	−15	6.46	16,308
R middle occipital gyrus (BA 19)	48	−72	9	1.74	540
L inferior temporal gyrus (BA 20)	−54	−57	−18	1.50	567
R supramarginal gyrus (BA 40)	57	−54	24	1.55	594
R posterior cingulate gyrus (BA 31)	3	−42	27	1.82	837
Increased activity					
Thalamus (medial dorsal nucleus)	0	−12	6	3.50	1,566
L posterior cerebellum (declive)	−42	−75	−27	3.48	4,050
R posterior cerebellum (declive)	12	−87	−27	3.38	17,901
L posterior cerebellum (tuber)	−36	−84	−39	3.72	3,024
R medial frontal gyrus/rectus (BA 11)	6	60	−18	4.29	999
L postcentral gyrus (BA 2)	−21	−39	72	1.96	837
L precuneus (BA 19)	−30	−81	39	3.08	3,284
R precuneus (BA 7)	9	−78	33	2.40	837
L superior parietal lobule (BA 7)	−29	−51	60	3.01	2,025
R inferior parietal lobule (BA 40)	66	−36	30	1.78	756
L middle temporal gyrus (BA 20)	−57	−33	−18	1.28	756
R middle temporal gyrus (BA 21)	69	−12	−6	2.29	6,210
L superior temporal gyrus (BA 41)/insula	−51	−27	6	2.29	1,701
R superior temporal gyrus (BA 22)/insula	48	−18	9	3.21	3,564
L superior temporal pole (BA 38)	−33	9	−36	2.58	4,860
R superior temporal pole (BA 38)	33	12	−30	4.26	1,485
R hippocampus (BA 21)	42	−9	−15	2.38	864

Abbreviations: BA, Brodmann area; fMRI, functional magnetic resonance imaging; MNI, Montreal Neurological Institute; PDRP–ALFF, Parkinson's disease–related spatial covariance pattern–amplitude of low-frequency fluctuation. The anatomic structures were defined from the covariance pattern in cohort A (see Figure 1A) in which the region weights were reliable at $P = 0.025$ according to the bootstrapping estimation on a voxel basis.

Table 2. Subject scores of PDRP–ALFF networks and ROC parameters in patients with PD and normal controls

	Subject scores		*ROC parameters*	
	Normal	*PD*	*AUC*	*Sensitivity/ specificity (%)*
Cohort A	*0.00 ± 0.14*	*2.02 ± 0.10*	*0.968 ± 0.013*	*91.4/88.9*
Cohort B	*0.00 ± 0.19*	*1.49 ± 0.09*	*0.921 ± 0.034*	*82.1/78.6*
Cohort C	0.55 ± 0.12	1.08 ± 0.08	0.782 ±0.061	70.0/69.2

Abbreviations: ALFF, amplitude of low-frequency fluctuation; AUC, the area under the curve; PDRP, Parkinson's disease–related pattern; ROC, receiver operating characteristic. Subject scores and AUC values are presented as mean ± s.e.m. The values marked in italics indicate the cohorts used to identify the PDRP–ALFF brain networks. In each cohort, subject scores for the corresponding brain network were elevated in the PD patients compared with the normal controls ($P < 0.00001$).

overlap, i.e., decreased activity in the SMA and occipital cortex, and increased activity in the thalamus and cerebellum but also exhibits important differences. For example, neural activity is decreased in the caudate nucleus and anterior putamen, and increased in the parietal cortex but does not change in the globus pallidus, sensorimotor cortex, and premotor areas in the PDRP from rsfMRI (Figure 1A). These differences should be due mostly to methodological factors. ^{18}F-fluorodeoxyglucose PET data measure synaptic neural activity via regional cerebral glucose metabolism, whereas ALFF may reflect the variability of local spontaneous neural activity in fMRI signal. The relationship between fMRI signal and FDG uptake is likely to be very complex and may be better understood by multimodal neuroimaging, neurophysiologic, and pathologic studies in animal models.

Several rsfMRI studies have investigated PD-related spontaneous neural activity or network connectivity.[12–18,27] These studies have provided useful information on understanding the neural correlates of clinical symptoms in PD, like tremor,[15] apathy, depression and motor dysfunction,[14] and cognitive impairment,[27] indicating that rsfMRI is useful in the investigation of neurophysiologic mechanisms underlying PD. Our findings further show that rsfMRI may be used to identify PDRP for possible assessment of network abnormality in individual subjects even though our study sample consisted mostly of patients at early to moderate stages.

Most regions in our PDRP–ALFF are involved in the corticobasal ganglia–thalamo–cortical loops, like the SMA, thalamus, caudate nucleus, putamen, temporal cortex, and limbic lobe, which include several parallel circuits such as sensorimotor, associative, and limbic circuits. The sensorimotor circuit projects somatotopically

© 2015 ISCBFM

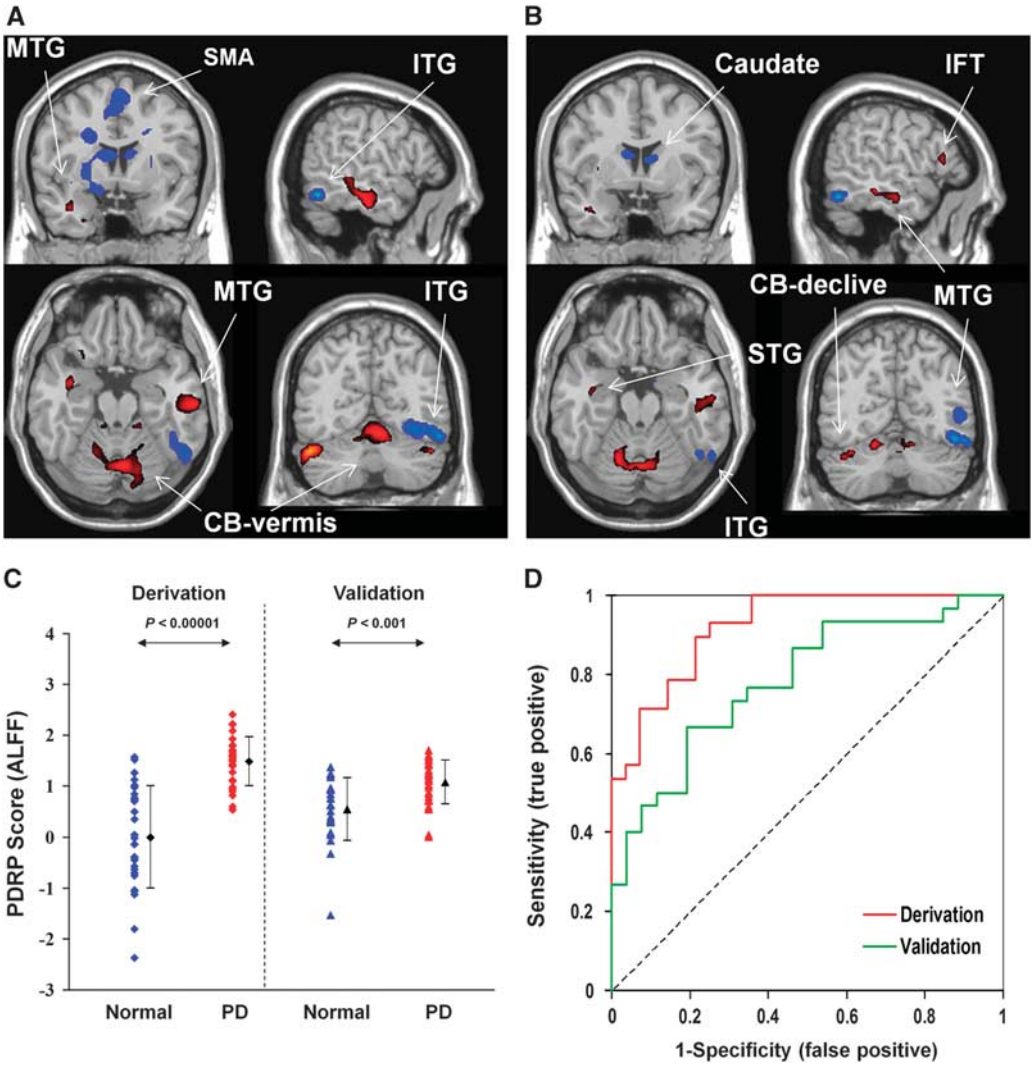

Figure 2. The comparison of Parkinson's disease–related spatial covariance pattern–amplitude of low-frequency fluctuation (PDRP–ALFF) brain networks and group discrimination in patients with PD and healthy controls in the split-sample analysis. (**A**) The pattern in the whole sample identified using ALFF images in cohort A was characterized by increased/decreased activity in the cortical and subcortical regions and reliable at $P < 0.025$ (Table 1). (**B**) The pattern in the split sample was derived using ALFF images from 28 PD patients and 28 normal controls in cohort B (reliable at $P < 0.05$) and validated prospectively in 30 PD patients and 26 normal controls in cohort C. (**C**) The expression of PDRP–ALFF from cohort B significantly discriminated the PD patients from the control subjects ($P < 0.001$) in both the derivation and validation cohorts. (**D**) Receiver operating characteristic curves for discriminating the PD patients from the normal controls. The discriminatory power was lower in cohort B and cohort C than that in cohort A (see Figure 1C). Both covariance patterns are overlaid on a standard T1-weighted magnetic resonance imaging (MRI) brain template and displayed side by side with a height threshold of ± 0.5 and an extent threshold of 30 voxels (240 mm^3). Red/blue color indicates increased/decreased covariation in local spontaneous neural activity among a large number of brain regions present in the PDRP. Error bars represent the s.d. plotted around the mean of each subject group. CB, cerebellum; IFT, inferior frontal triangular parts; ITG, inferior temporal gyrus; MTG, middle temporal gyrus; SMA, supplementary motor area; STG, superior temporal gyrus.

from the primary motor cortex, premotor area, and SMA to the putamen, then through the thalamus projects back to these cortical motor areas.[28] The dysfunction of the sensorimotor circuit has been reported to cause motor difficulties in PD, like akinesia and bradykinesia.[29] The associative circuit projects from associative cortical areas, like the prefrontal cortex, and the temporal regions to the caudate nucleus and the putamen,[30] whereas the limbic circuit projects from the limbic cortices, the amygdala and the hippocampus to the ventral striatum.[31] It has been shown that some nonmotor signs in PD, like cognitive decline, could be linked to the reduced ^{18}F-fluorodopa uptake in the associative circuit,[32] as well as in the limbic circuit.[33]

The PDRP–ALFF reported in this study also contains areas outside the corticobasal ganglia–thalamo–cortical loops, e.g., the cerebellum. The cerebellum is known to influence motor and cognitive operations via the cerebello–thalamo–cortical circuit.[34] Increasing evidence suggests that this circuit is an important mechanism underlying pathophysiology of the PD resting tremor.[15,35] However, as all patients in this study have mild tremor at most, the results reported here were not likely to be influenced by the factors related to resting tremor. The increased activity in the cerebellum is possibly a compensation for basal ganglia dysfunction.[36]

The PDRP–ALFF expression from rsfMRI showed a high accuracy of ~90% to discriminate PD patients from healthy controls in the large sample of cohort A (91% sensitivity and 89% specificity). Despite methodological differences between studies this finding was in line with several previous reports,[13,18] suggesting that

© 2015 ISCBFM

rsfMRI could be potentially useful for differentiating PD patients from healthy controls at an individual level. Although the subject scores of the PDRP–ALFF did not change with regard to gender and age in the normal controls, they were higher in men and correlated positively with age in the patients. The latter confirmed with our patient sample in which men were slightly older and had marginally more severe motor symptoms than women.

We assessed the reproducibility of PDRP–ALFF in the split-sample analysis, which gave rise to a topographic pattern very similar to that from the entire cohort. Pattern expression was abnormally elevated ($P < 0.001$) in PD patients in both the derivation and prospective validation samples, but with inferior group discrimination (Figure 2; Table 2) compared with the large sample in cohort A. We found that voxel weights on this ALFF-derived pattern had different degrees of reliability relative to those for the analogous PET–derived topography (ALFF: $P < 0.05$; PET: $P < 0.001$; bootstrap resampling estimation).[3] In addition, the smaller group difference in pattern expression in both samples resulted in a lower accuracy for single-case classification. Relative to the corresponding results obtained with FDG PET imaging, these performance metrics were similar to the finding in a smaller sample of predominately hemi-PD patients,[8] but worse than those achieved consistently in both derivation and validation samples of comparable sizes and patient characteristics.[3,4] Of note, the discrimination power of the PDRP–ALFF derived in the entire sample of cohort A was lower but approaching that from FDG PET with smaller sample sizes (sensitivity/specificity $\geqslant 93\%$) despite the equally low reliability of PDRP–ALFF. Such differences could be attributed mainly to lower signal-to-noise ratio characteristics of fMRI relative to FDG PET on the level of individual basis. Nonetheless, these results suggest that accurate discrimination of PD is likely by assessing subject score prospectively using PDRP–ALFF derived from a large sample (e.g., cohort A) as described above.

Research over the last decade has shown that FDG PET and fMRI provide unique and complementary information in measuring changes in local neural activity. Despite currently inferior signal-to-noise ratio compared with FDG PET, fMRI modality does offer several unique advantages. In addition to higher spatial and temporal resolutions, MRI scanners are more widely available and do not involve ionizing radiation. This allows a single subject to be scanned repeatedly, and more subjects to be scanned to increase statistical power. Compared to the conventional task-based fMRI methods, rsfMRI is easy to perform and not too demanding on the participants, and can circumvent task-related confounds, increase signal-to-noise ratio, and expand patient populations. It is now possible to use rsfMRI to evaluate neuronal activity instead of FDG PET as shown by many studies cited in this paper and elsewhere (see the reviews by Prodoehl *et al*[37] and Fox and Raichle[38]). Our findings highlight the feasibility of using rsfMRI to identify and validate disease-related spatial covariance topographies. However, major efforts are still needed to optimize the stability and accuracy of disease-related patterns derived using this imaging method. Additional work may also be necessary to conduct FDG PET and rsfMRI in the same cohort of patients to compare the performance of each measure as an optimal biomarker in PD.

It is unclear whether our findings can be generalized to all PD patients because of some limitations in this study. First, our patients had mild tremor at most to facilitate rsfMRI. The FDG PET study has shown that tremor-dominant PD patients have a distinct spatial covariance pattern of regional cerebral glucose metabolism.[35] Further rsfMRI studies are necessary to explore tremor-related spatial covariance pattern of brain activity. Second, our patients exhibited typical motor symptoms of rigidity and bradykinesia mostly at early to moderate stages. This narrow range of disease severity resulted in part from the recruitment of a large PD cohort with mild tremor. Extensive work in parkinsonian patients at early stage, and with atypical symptoms is still needed before rsfMRI can be used as a biomarker to identify PD patients at an individual level. It is also necessary to examine the relationship between the PDRP–ALFF scores and clinical symptoms by studying patients with a wide spread of UPDRS motor ratings or Hoehn and Yahr stages. Third, nonmotor symptoms like cognitive, psychiatric, and emotional impairments were not examined in our patients. It is well recognized that nonmotor problems are present in most PD patients and their neuroimaging correlates can be assessed by rsfMRI.[14] Thus, the influences of these nonmotor symptoms on PDRP and corresponding cognitive-related patterns need to be investigated in the future.

An inherent limitation in using rsfMRI on PD is that tremor can disturb fMRI signal. Thus, up to now, most fMRI studies have excluded patients with obvious tremor. Some improvement in data acquisition and analysis can be helpful in overcoming this problem. For example, simultaneous electromyography monitoring during scanning is helpful to regress out the influence of tremor on fMRI signal. Motion correction during data analysis also has benefits in reducing movement artifacts. With continued improvement in imaging and data analysis techniques, the application of rsfMRI to tremor-dominant PD is increasingly becoming feasible.

In summary, we have shown that rsfMRI can be used for identification of disease-related covariance patterns, and has the potential for differentiation of PD patients from healthy controls on a single-case basis. It is critically important to further develop and validate this technique, and optimize imaging protocols ranging from innovations in coil design and acquisition sequences/parameters to advances in signal-processing strategies and data analytical methodologies. Further studies are needed to test the replicability of PDRP–ALFF prospectively in new patient samples, validate its test–retest stability and reproducibility with different MRI scanners, and assess its clinical correlation and modulation by antiparkinsonian therapies. Such comprehensive technical improvement in the rsfMRI method and more rigorous validation in independent patient populations can be helpful for establishing a simple and noninvasive imaging biomarker for PD and related disorders.

AUTHOR CONTRIBUTIONS

TW was involved in conception, organization, and execution of the research; writing of the first draft, review, and critique of the manuscript. YM participated in conception of the research, analysis of the data, review, and critique/revision of the manuscript. ZZ was involved in analysis of the data. SP was responsible for network analysis of the data and preparation of the results. XW was involved in execution of the research. DE gave valuable suggestions on the design of data analysis strategy and was responsible for the revision of the manuscript. PC was involved in conception of the research.

DISCLOSURE/CONFLICT OF INTEREST

The authors declare no conflict of interest.

REFERENCES

1 Adler CH, Beach TG, Hentz JG, Shill HA, Caviness JN, Driver-Dunckley E *et al*. Low clinical diagnostic accuracy of early vs advanced Parkinson disease: clinicopathologic study. *Neurology* 2014; **83**: 406–412.
2 Ma Y, Tang C, Spetsieris PG, Dhawan V, Eidelberg D. Abnormal metabolic network activity in Parkinson's disease: test-retest reproducibility. *J Cereb Blood Flow Metab* 2007; **27**: 597–605.
3 Poston KL, Eidelberg D. Network biomarkers for the diagnosis and treatment of movement disorders. *Neurobiol Dis* 2009; **35**: 141–147.
4 Wu P, Wang J, Peng S, Ma Y, Zhang H, Guan Y *et al*. Metabolic brain network in the Chinese patients with Parkinson's disease based on (18)F-FDG PET imaging. *Parkinsonism Relat Disord* 2013; **19**: 622–627.

© 2015 ISCBFM

5 Asanuma K, Tang C, Ma Y, Dhawan V, Mattis P, Edwards C *et al.* Network modulation in the treatment of Parkinson's disease. *Brain* 2006; **129**: 2667–2678.
6 Feigin A, Kaplitt MG, Tang C, Tang C, Lin T, Mattis P *et al.* Modulation of metabolic brain networks after subthalamic gene therapy for Parkinson's disease. *Proc Natl Acad Sci USA* 2007; **104**: 19559–19564.
7 Tang CC, Poston KL, Eckert T, Feigin A, Frucht S, Gudesblatt M *et al.* Differential diagnosis of parkinsonism: a metabolic imaging study using pattern analysis. *Lancet Neurol* 2010; **9**: 149–158.
8 Teune LK, Renken RJ, Mudali D, De Jong BM, Dierckx RA, Roerdink JB *et al.* Validation of parkinsonian disease-related metabolic brain patterns. *Mov Disord* 2013; **28**: 547–551.
9 Eckert T, Van Laere K, Tang C, Lewis DE, Edwards C, Santens P *et al.* Quantification of Parkinson's disease-related network expression with ECD SPECT. *Eur J Nucl Med Mol Imaging* 2007; **34**: 496–501.
10 Ma Y, Huang C, Dyke JP, Pan H, Alsop D, Feigin A *et al.* Parkinson's disease spatial covariance pattern: noninvasive quantification with perfusion MRI. *J Cereb Blood Flow Metab* 2010; **30**: 505–509.
11 Melzer TR, Watts R, MacAskill MR, Pearson JF, Rüeger S, Pitcher TL *et al.* Arterial spin labelling reveals an abnormal cerebral perfusion pattern in Parkinson's disease. *Brain* 2011; **134**: 845–855.
12 Wu T, Long X, Zang Y, Wang L, Hallett M, Li K *et al.* Regional homogeneity changes in patients with Parkinson's disease. *Hum Brain Mapp* 2009; **30**: 1502–1510.
13 Skidmore FM, Yang M, Baxter L, von Deneen KM, Collingwood J, He G *et al.* Reliability analysis of the resting state can sensitively and specifically identify the presence of Parkinson disease. *Neuroimage* 2013; **75**: 249–261.
14 Skidmore FM, Yang M, Baxter L, von Deneen K, Collingwood J, He G *et al.* Apathy, depression, and motor symptoms have distinct and separable resting activity patterns in idiopathic Parkinson disease. *Neuroimage* 2013; **81**: 484–495.
15 Helmich RC, Janssen MJ, Oyen WJ, Bloem BR, Toni I. Pallidal dysfunction drives a cerebellothalamic circuit into Parkinson tremor. *Ann Neurol* 2011; **69**: 269–281.
16 Wu T, Wang L, Chen Y, Zhao C, Li K, Chan P. Changes of functional connectivity of the motor network in the resting state in Parkinson's disease. *Neurosci Lett* 2009; **460**: 6–10.
17 Wu T, Long X, Wang L, Hallett M, Zang Y, Li K *et al.* Functional connectivity of cortical motor areas in the resting state in Parkinson's disease. *Hum Brain Mapp* 2011; **32**: 1443–1457.
18 Szewczyk-Krolikowski K, Menke RA, Rolinski M, Duff E, Salimi-Khorshidi G, Filippini N *et al.* Functional connectivity in the basal ganglia network differentiates PD patients from controls. *Neurology* 2014; **83**: 208–214.
19 Lang A, Fahn S. Assessment of Parkinson's disease. Munsat TL (ed). *Quantification of Neurological Deficit*. Butterworths: Boston, 1989; pp 285–309.
20 Hoehn MM, Yahr MD. Parkinsonism: onset, progression and mortality. *Neurology* 1967; **17**: 427–442.
21 Hou Y, Wu X, Hallett M, Chan P, Wu T. Frequency-dependent neural activity in Parkinson's disease. *Hum Brain Mapp* 2014; **35**: 5815–5833.
22 Biswal B, Yetkin FZ, Haughton VM, Hyde JS. Functional connectivity in the motor cortex of resting human brain using echo-planar MRI. *Magn Reson Med* 1995; **34**: 537–541.
23 Zang YF, He Y, Zhu CZ, Cao QJ, Sui MQ, Liang M *et al.* Altered baseline brain activity in children with ADHD revealed by resting-state functional MRI. *Brain Dev* 2007; **29**: 83–91.
24 Habeck C, Fosterb NL, Perneczkyc R, Kurz A, Alexopoulos P, Koeppe RA *et al.* Multivariate and univariate neuroimaging biomarkers of Alzheimer's disease. *Neuroimage* 2008; **40**: 1503–1515.
25 Eidelberg D. Metabolic brain networks in neurodegenerative disorders: a functional imaging approach. *Trends Neurosci* 2009; **32**: 548–557.
26 Spetsieris PG, Eidelberg D. Scaled subprofile modeling of resting state imaging data in Parkinson's disease: methodological issues. *Neuroimage* 2011; **54**: 2899–2914.
27 Baggio HC, Sala-Llonch R, Segura B, Marti MJ, Valldeoriola F, Compta Y *et al.* Functional brain networks and cognitive deficits in Parkinson's disease. *Hum Brain Mapp* 2014; **35**: 4620–4634.
28 DeLong MR, Wichmann T. Circuits and circuit disorders of the basal ganglia. *Arch Neurol* 2007; **64**: 20–24.
29 Grafton ST. Contributions of functional imaging to understanding parkinsonian symptoms. *Curr Opin Neurobiol* 2004; **14**: 715–719.
30 Selemon LD, Goldman-Radic PS. Longitudinal topography and interdigitation of cortico-striatal projects in the rhesus monkey. *J Neurosci* 1985; **5**: 776–794.
31 Graybiel AM, Aosaki T, Flaherty AW, Kimura M. The basal ganglia and adaptive motor control. *Science* 1994; **265**: 1826–1831.
32 Rinne JO, Portin R, Ruottinen H, Nurmi E, Bergman J, Haaparanta M *et al.* Cognitive impairment and the brain dopaminergic system in Parkinson disease: [18F]fluorodopa positron emission tomographic study. *Arch Neurol* 2000; **57**: 470–475.
33 Ito K, Saito AN, Kato T, Arahata Y, Nakamura A, Kawasumi Y *et al.* Striatal and extrastriatal dysfunction in Parkinson's disease with dementia: a 6-[(18)]fluoro-L-dopa PET study. *Brain* 2002; **125**: 1358–1365.
34 Middleton FA, Strick PL. Cerebellar projections to the prefrontal cortex of the primate. *J Neurosci* 2001; **21**: 700–712.
35 Mure H, Hirano S, Tang CC, Isaias IU, Antonini A, Ma Y *et al.* Parkinson's disease tremor-related metabolic network: characterization, progression, and treatment effects. *Neuroimage* 2011; **54**: 1244–1253.
36 Wu T, Hallett M. The cerebellum in Parkinson's disease. *Brain* 2013; **136**: 696–709.
37 Prodoehl J, Burciu RG, Vaillancourt DE. Resting state functional magnetic resonance imaging in Parkinson's disease. *Curr Neurol Neurosci Rep* 2014; **14**: 448.
38 Fox MD, Raichle ME. Spontaneous fluctuations in brain activity observed with functional magnetic resonance imaging. *Nat Rev Neurosci* 2007; **8**: 710–711.

© 2015 ISCBFM